 CMC, vol.56, no.3, pp.517-527, 2018

# In Situ Synthesis of Cuprous Oxide/Cellulose Nanofibers Gel and Antibacterial Properties

**Ying Hu[1, 2], Qinfei Ke[1], Zhe Li[2], Wanli Han[3] and Zhiyong Yan[2, *]**

**Abstract:** Cellulose nanofibers were synthesized by *acetobacter xylinum* (*xylinum 1.1812*). The cellulose nanofibers with 30-90 nm width constructed three-dimension network gel, which could be used as a wound dressing since it can provide moist environment to a wound. However, cellulose nanofibers have no antimicrobial activity to prevent wound infection. To achieve antimicrobial activity, the cellulose nanofibers can load cuprous oxide ($Cu_2O$) particles on the surface. The cuprous oxide is a kind of safe antibacterial material. The copper ions can be reduced into cuprous oxides by reducing agents such as glucose, $N_2H_4$ and sodium hypophosphite. The cellulose nanofibers network gel was soaked in $CuSO_4$ solution and filled with copper ions. The cuprous oxide nanoparticles were in situ synthesized by glucose and embedded in cellulose nanofibers network. The morphologies and structure of the composite gel were analyzed by FESEM, FTIR, WAXRD and inductively coupled plasma (ICP). The sizes of $Cu_2O$ embedded in cellulose nanofibers network are 200-500 nm wide. The peak at 605 $cm^{-1}$ attributed to Cu(I)-O vibration of $Cu_2O$ shits to 611 $cm^{-1}$ in the $Cu_2O$/ cellulose composite. The $Cu_2O$/ cellulose nanofibers composite reveals the obvious characteristic XRD pattern of $Cu_2O$ and the results of ICP show that the content of $Cu_2O$ in the composite is 13.1%. The antibacterial tests prove that the $Cu_2O$/ cellulose nanofibers composite has the high antibacterial activities which is higher against S. aureus than against E. coli.

**Keywords:** Cellulose nanofiber, cuprous oxide, in situ synthesis, antibacterial.

## 1 Introduction

Above 15 million people died of the infectious diseases every year in the world [Sunada, Minoshima and Hashimoto (2012)]. The bacteria infect the patients from person-to-person on their surface of organs and skins. It is very necessary to kill the bacteria on the skins and the surrounding environment by using antibacterial materials. The antibacterial materials exposed to the surface can inactivate viral particles in the environment, prevent viral transmitting and thereby lower the risks of infections. A number of inorganic

[1] Engineering Research Center of Technical Textiles, Donghua University, Shanghai, 201620, China.

[2] Key Laboratory of Yarn Material Manufacturing and Processing of Zhejiang Province, Jiaxing University, Jiaxing, 314001, China.

[3] School of Materials Science and Engineering, Georgia Institute of Technology, Atlanta, 30318, USA.

[*] Corresponding Author: Zhiyong Yan. Email: yzyong77@mail.zjxu.edu.cn.

materials such as zinc, copper, silver and their oxides could be often used as antiviral and antibacterial materials [Khatami, Heli, Jahani et al. (2017); Ma, Guo, Guo et al. (2015); Rezaie, Montazer, Rad et al. (2017)]. The silver nanoparticles are cytotoxic and genotoxic, and should be limited to use in materials contacted with human organs. Copper has been used as antibacterial materials since ancient times, however, some experiment results reveal that the cuprous oxides ($Cu_2O$) have superior antibacterial activities because of their activity mechanism different from silver nanoparticles, moreover, the cuprous oxides have no toxic to human organs and low-cost in manufacture [She, Wan, Tang et al. (2016); Yang, Li, Lin et al. (2016)].

$Cu_2O$ has unique physical and chemical properties and has attracted extensive interest to use as solar energy conversion, catalysis, gas sensors, photocatalysts and antibacterial materials. Many methods are created to synthesize different morphology and size $Cu_2O$ and a series of different $Cu_2O$ shapes including cubes, octahedrons, polyhedrons, nanocubes, hollow structures, nanowires, flower-like, hex-pod-like and hexapods have been synthesized [Xu, Chen, Jiao et al. (2007); Xu, Yi, Fen et al. (2003)]. The sizes of $Cu_2O$ have a great influence on their properties. The research results show that the antibacterial properties depend on the morphologies and sizes [Li, Ni, Yu et al. (2014); Pang, Gao and Lu (2009)]. The cuprous oxide nanoparticles are prone to aggregate, due to an der Waals forces between nanoparticles and highly surface energy, which decreases their specific surface area and antibacterial activities. It is necessary to disperse the cuprous oxide nanoparticles in order to enlarge their superiorities of high specific surface area and antibacterial activities. It is a good method to fix the cuprous oxide nanoparticles on the solid surface. Cellulose nanofibers are the excellent materials to load the inorganic nanoparticles, due to a large number of hydrophilic hydroxyl groups on the surface of cellulose nanofibers, which can interact with the electrons on the inorganic nanoparticles and absorb firmly the nanoparticles [Khalid, Khan, Ul-Islam et al. (2017); Xiang and Acevedo (2017); Zhang, Tang, Yang et al. (2016)].

Cellulose nanofibers can be used as medical tissues and received extensive attention. Several bacteria including *Gluconacetobacter*, *Sarcina and Agrobacterium* can metabolism and secrete cellulose nanofibers named bacterial cellulose (BC) [Keskin, Urkmez and Hames (2017); Pita, Pinto and Lira (2015); Sepulveda, Valente, Reis et al. (2016)]. The nanofibers interwoven into three-dimensional network gel, resulting in numerous micropores with porosity and high water-holding ability. The microporous network can provide place to load the cuprous oxide particles. In order to disperse uniformly the nanoparticles, it is a very efficient method to in situ synthesize using the precursors of nanoparticles.

In this work, the cuprous oxide particles were in situ synthesized in the cellulose nanofibers three-dimensional network gel. The sizes and morphologies of cuprous oxide particles were controlled by adjusting the pH of solution, temperature and glucose concentration. The chemical and physical structure was characterized by FTIR, XRD and SEM. The composite gel showed the higher antibacterial activities.

## 2 Materials and methods

### *2.1 Culture methods and cellulose nanofibers biosynthesis*

*G. xylinum 1.1812* (*ATCC 23767*) strains were given by the Institute of Microbiology, Chinese Academy of Sciences. The lyophilized strains powder was first dissolved in pH=6.0 nutrient medium (0.5 w/v% peptone, 0.5 w/v% yeast extract, 0.2 w/v% sodium phosphate dibasic, 5 w/v% glucose, 0.1 w/v% citric acid and 0.1w/v% potassium dihydrogen phosphate). After cultivated for 24 h at 28°C, a layer of pellicle floated on surface. The clear solution centrifugated was then inoculated into square culture dish (13 cm*13 cm) with the volume of 50 mL nutrient ingredients medium which was sterilized at 121°C for 30 min by autoclaving. 7 days later, the culture medium was changed into a gel. The gel was boiled in 1% sodium hydroxide solution for 30 min to remove the cells and medium embedded in the cellulose, then rinsed with deionized water for 3 days until pH=7 of the rinsed solution and freeze-dried at -30°C.

### *2.2 Preparation of the $Cu_2O$ /cellulose nanofibers composite gel*

The rinsed cellulose gel (5 cm×10 cm) were dried in the air for 1 day. 25 g copper sulfate ($CuSO_4$•$5H_2O$) was dissolved in 250 mL in deionized water to get copper sulfate solution, 20 g glucose was dissolved in 100 deionized water to get glucose solution and 40 g NaOH was dissolved in 100 deionized water to get NaOH solution. The composite gel samples were prepared as following: first, measuring copper sulfate solution and glucose solution, mixing them into uniform and transparent solution; then the cellulose gels were soaked in the $CuSO_4$/glucose solution and ultrasound for 24 h in order to make $CuSO_4$ and glucose fill the pores among nanofibers; then the above solution was laid in heated water bath and added NaOH solution dropwise, stirring for 1 h. The reaction parameters were listed in Tab. 1. The red gel was taken out of the solution and cut into 5 cm*10 cm sheet, stored at 4°C until further usage. After the remaining solution was centrifuged, the brick red precipitate was obtained and freeze-dried.

**Table 1:** The experimental parameters of the samples

| Sample | Water (mL) | $CuSO_4$ (mol) | Glucose (mol) | NaOH (mol) | T (°C) | Time (h) |
|---|---|---|---|---|---|---|
| 1 | 100 | 0.005 | 0.005 | 0.03 | 70 | 1 |

### *2.3 Field emission scanning electron microscopy (FESEM)*

Field emission scanning electron microscopy (FE-SEM, Hitachi S-4800) was performed at 10 kV to determine the microstructures and morphologies of the composites. All the samples were freeze-dried and sputter-coated with a thin layer of gold power before microscopic observation.

### *2.4 Fourier transform infrared (FTIR) spectroscopy*

The freeze-dried cellulose nanofibers samples were placed across a hole in a magnetic holder. FTIR spectra were recorded on a Nicolet model 6000C equipped with a MCT detector in the absorption mode with a resolution of 2 $cm^{-1}$ in the range of 4000~400 $cm^{-1}$.

### *2.5 Wide-angle X-ray diffractometry (WAXRD)*

X-ray diffraction (XRD) (EQuniox 3000, INEL) with Cu Kα radiation source (λ=1.5418 Å) was used to evaluate the presence and phases of nanoparticles loaded on the cellulose nanofibers. The diffraction profile was processed by computer-aided fitting analysis and transformed to basic crystallographic features: D-spaces of equatorial lattice planes. The crystalline siz ($D_{(hkl)}$) could be calculated according to the each corresponding peaks in XRD patterns (Eq. (1)) [Oh, Yoo, Shin et al. (2005)]:

$$D_{(hkl)}=0.9\ \lambda/\beta\cos\theta \tag{1}$$

where β, λ and θ are full width at half maximum, *X*-ray wavelength and the diffraction angle, respectively.

### *2.6 Antibacterial activity test*

In order to investigate the antimicrobial ability of composite gel, the gel was punched into circle gels of the diameter of 1.0 cm. S. aureus as representative of Gram-positive bacterium and E. coli and as representative of Gram-negative bacterium were selected as test strains. All the disks and materials were sterilized in an autoclave before experiments, and experimental operations were conducted in the super clean bench. Firstly, the melted sterilized LB agar medium was poured into petri dishes and then solidified. Secondly, the medium containing bacteria ($10^8$ CFU/mL) was uniformly layered over LB agar plates. Thirdly, the circle composite gels were gently placed on the lawn of bacteria in LB agar plates. To compare the antibacterial properties, one piece of pure cellulose gel and two pieces of composite gels were placed on the same LB agar plates. After the plates were cultivated at 28°C for 24 h, the morphologies of bacteria in and out of inhibition zone were observed by SEM.

### *2.7 Inductively coupled plasma optical emission spectrometer (ICP-OES) test*

To determine the content of $Cu_2O$ in composite gel, the composite gels were vacuum-dried. Then the samples were dissolved in a mixed solution of concentrated $HNO_3$/H. Inductively coupled plasma optical emission spectrometer (ICP-OES) (Optima 5300 DV), was used to analyze the concentration of the Cu element.

## 3 Result and discussion

### *3.1 Morphology of cellulose nanofibers gel*

The photograph of the cellulose gel produced at 28°C is shown in Fig. 1. It is a milky white gel membrane with the thickness of about 10 mm. The surface and bottom of the gel are smooth.

**Figure 1:** Photograph of cellulose nanofibers gel

### *3.2 Reactional mechanism*

The color of the solution gradually turn to light turbid blue, dark blue, and brick red from blue clarification with the increase of the heating time, shown as Fig. 2. Fig. 2a shows the gel soaked in the blue $CuSO_4$ solution and the cellulose gel filled by $Cu^{2+}$ and $SO_4^{2-}$ ions is light blue. Fig. 2b shows the brick red suspension after heating 1 h and the cellulose gel is yellowish red, shown as Fig. 2c.

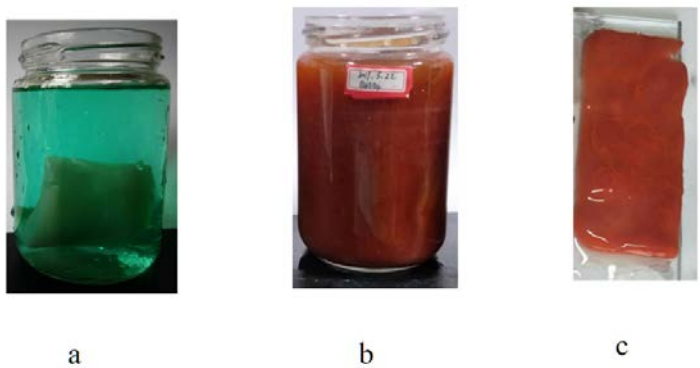


**Figure 2:** Photographs of cellulose nanofibers/$CuSO_4$ mixture solution (a), brick red solution after heated 1 h (b) and the brick red composite gel (c)

The change of the color of the gel is attributed to the $Cu^{2+}$ induced gradually by glucose, which can be described as the chemical Eqs. (1), (2) and (3) [Yang, Li, Lin et al. (2016)]:

$$CuSO_4 \cdot 5H_2O\ (aq) + 2NaOH\ (aq) \rightarrow Cu(OH)_2 + Na_2SO_4\ (aq) + 5H_2O \quad (2)$$

$$Cu(OH)_2\ (aq) + 2OH^-\ (aq) \rightarrow [Cu(OH)_4]^{2-}\ (aq) \quad (3)$$

$$[Cu(OH)_4]^{2-}(aq) + C_5H_{11}O_5\text{-}CHO\ (aq) + NaOH(aq) \rightarrow Cu_2O(s) + C_5H_{11}O_5COONa\ (aq) + 2H_2O \quad (4)$$

The dark blue $Cu(OH)_2$ suspension is changed into brick red precipitate which may be $Cu_2O$ according to the chemical reaction equations.

The shapes and sizes of $Cu_2O$ depend on the reaction conditions. Fig. 3a illustrates that the $Cu_2O$ particles reduced from the $Cu^{2+}$ ions in the $CuSO_4$ solution are the quasi-octahedron with the width of 600-900 nm. Fig. 3b reveals that the cellulose nanofibers are 30-90 nm wide and assemble into three-dimensional network layer-by-layer, which leaves a lot of micropores in the network. The sizes of $Cu_2O$ embedded in cellulose nanofibers network are 200-500 nm wide and irregular, as shown in Fig. 3c. The $Cu_2O$ particles and cellulose nanofibers interpenetrate, indicating that the $Cu^{2+}$ ions are adsorbed in the cellulose nanofibers before reduced. The reactional processing can be manifested as Fig. 4. The copper ions were uniformly filled with the whole cellulose gel, then reduced into the precipitate of $Cu_2O$ which were uniformly dispersed in the gel.

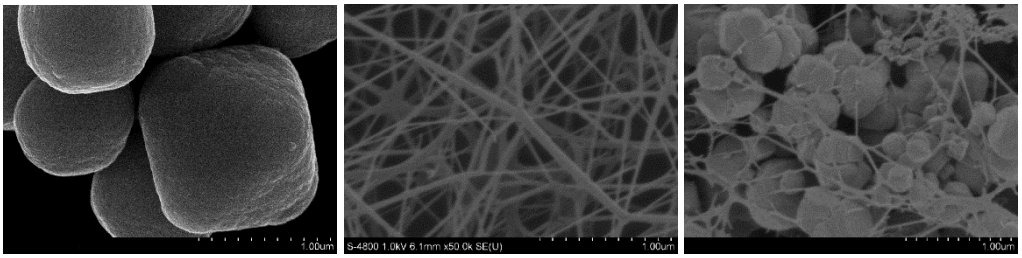

a b c

**Figure 3:** SEM images of $Cu_2O$ reduced from $Cu^{2+}$ in the $CuSO_4$ solution (a), cellulose nanofibers (b) and $Cu_2O$/cellulose nanofiber composites (c)

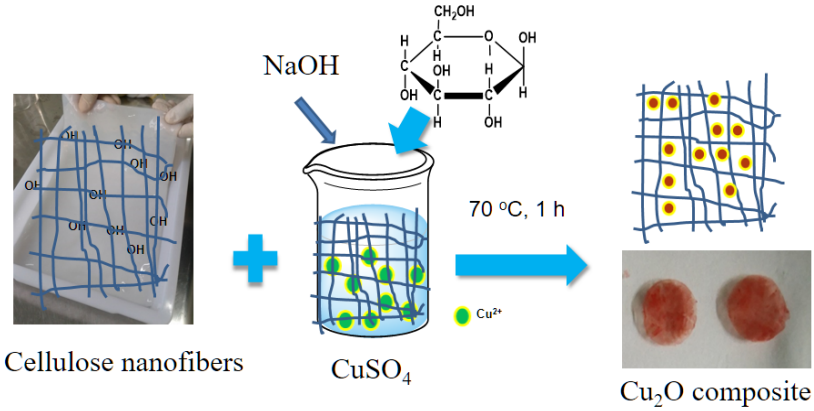


**Figure 4:** The schematic representation of the $Cu_2O$/cellulose nanofibers composite via in situ synthesis

### *3.3 FTIR*

The FTIR spectra of $Cu_2O$, cellulose nanofibers and $Cu_2O$/cellulose nanofibers composite are presented in Fig. 5. A weak band at 458 $cm^{-1}$ is assigned to the metal-oxygen vibrational bond. Cellulose nanofibers and $Cu_2O$/cellulose nanofibers composite both reveal the characteristic peaks of cellulose molecules. The strong peak at 3349 $cm^{-1}$ attributed to the intra-molecular hydrogen bonds for (3)O-H-O(5), as shown in Fig. 5a, however, the intensity of peak at 3349 $cm^{-1}$ in nanofibers is higher and sharper than that in the composite, which may be ascribed to the $Cu_2O$ particles in the network disrupting the interaction between the cellulose nanofibers. Fig. 5b brings out the spectra from 700 $cm^{-1}$ to 400 $cm^{-1}$. The difference is very obvious near 600-620 $cm^{-1}$. The peak at 605 $cm^{-1}$ is related to Cu(I)-O vibration of $Cu_2O$ particles [Sedighi, Montazer and Samadi (2014)]. In the $Cu_2O$/cellulose nanofibers composite, the peak shifts from 605 $cm^{-1}$ to 611 $cm^{-1}$ and the peak at 619 $cm^{-1}$ disappear, which exists in cellulose. The change of wavenumber near 605 $cm^{-1}$ manifest the Cu-O and cellulose molecules interact, as the change of peaks at 3349 $cm^{-1}$.

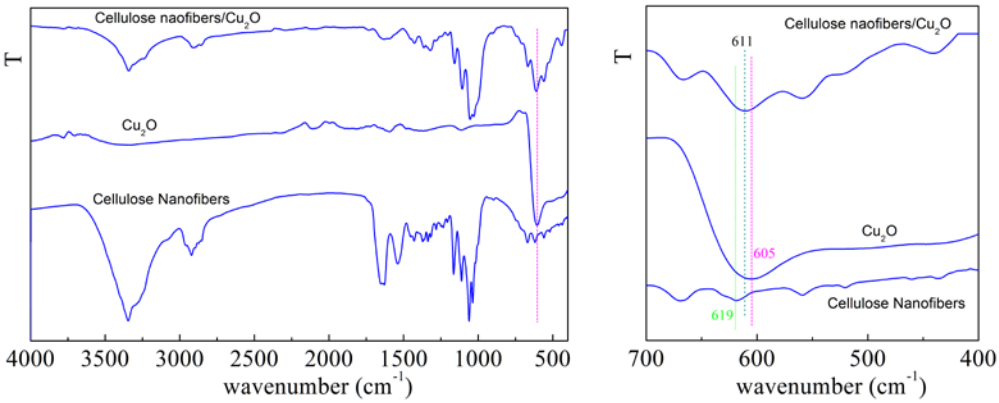


a b

**Figure 5:** FTIR spectra of 4000-400 $cm^{-1}$(a) and 700-400 $cm^{-1}$ (b)

### *3.4 XRD*

The WAXRD patterns of BC nanofibers, $Cu_2O$ and $Cu_2O$/BC nanofibers composites are shown in Fig. 6. The $Cu_2O$ samples reduced from the $Cu^{2+}$ ions in the $CuSO_4$ solution reveal the sharp characteristic diffraction peaks of $Cu_2O$ at 29.2°, 36.0°, 41.9°, 61.1°, 73.3° and 77.3° corresponding to the (110), (111), (200), (220), (311) and (222) planes, respectively [Chen, Chen, Xue et al. (2002)], which indicates that the $Cu_2O$ samples are pure, no CuO and Cu. The pattern of cellulose nanofibers reveals the diffraction peaks at 14.4°, 16.6° and 22.7°, corresponding to the crystallographic plane of $(11\bar{0})$, (110) and (200), respectively. The patter of $Cu_2O$/cellulose nanofibers composite only reveals the characteristic diffraction peaks of cellulose at 22.7°, and the peaks at 14.4° and 16.6° disappear. However, the characteristic peaks of $Cu_2O$ are obviously shown in the pattern of $Cu_2O$/cellulose nanofibers composite, which may be related to a large number of $Cu_2O$ particles deposited on the surface of composite, as the brick red color is displayed. According to Eq. (1) at 36.5°, the $D_{(hkl)}$ of $Cu_2O$ reduced from the $Cu^{2+}$ ions in the $CuSO_4$ solution is 28.6 nm, while the value of the composite is 11.8 nm. The crystalline size of $Cu_2O$ reduced from the $Cu^{2+}$ ions in the $CuSO_4$ solution is larger than that of $Cu_2O$ embedded in the composite, which is consistent with the results of SEM images. The difference of crystalline size between $Cu_2O$ and the composite demonstrates that $Cu_2O$ in the $CuSO_4$ solution could grow freely; $Cu_2O$ embedded in the network are constricted by limited space and the interaction of chemical bands between $Cu_2O$ and -OH groups in cellulose molecules, difficult to grow freely.

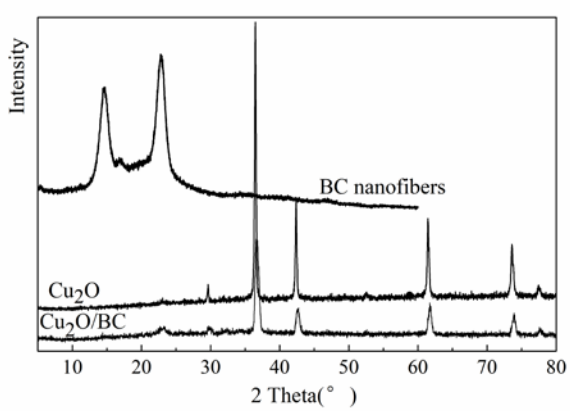


**Figure 6:** WAXRD patterns of BC nanofibers, $Cu_2O$ and $Cu_2O$/BC nanofibers composites

### *3.5 Antibacterial activity test*

The antibacterial properties of $Cu_2O$/cellulose nanofibers composite was examined against both E. coli and S. aureus bacteria using disc diffusion method (zone of inhibition test). In order to reduce the test error, every disc is placed two pieces of $Cu_2O$/cellulose composite gels. Figs. 7a and 7b present the shapes and size of the inhibition zone of E. coli and S. aureus, respectively. The halo diameter of nanofibers/$Cu_2O$ composite is 38 mm against E. coli while 43 mm against S. aureus. The composite exhibits efficient antibacterial activity due to their large surface area loaded on the surface of cellulose nanofibers. Relatively, the composite reveals higher antibacterial efficient against S. aureus than E. coli. Moreover, the color of composite becomes very light than that before antibacterial test and the brick red color of $Cu_2O$ vanishes. It may be reasonable that the $Cu_2O$ particles are changed into $Cu^{2+}$ ions which diffuse into the agar medium. The color of composite against S. aureus is lighter than against E. coli, indicating that the more $Cu_2O$ particles against S. aureus diffuses into the medium, which demonstrates higher antibacterial activity than those against E. coli.

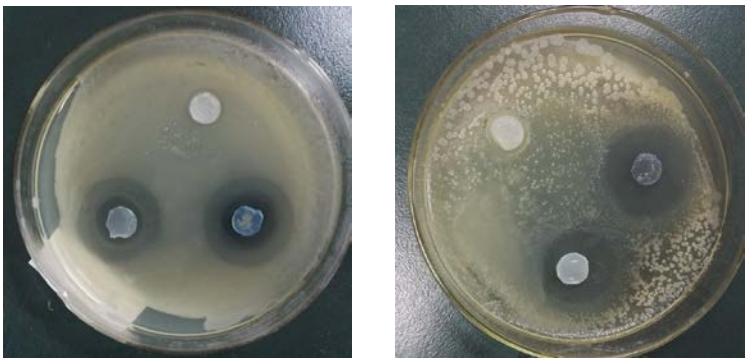

a b

**Figure 7:** Inhibition zone test of $Cu_2O$/cellulose nanofibers composite and cellulose nanofibers against E. coli (a) and S. aureus (b)

Fig. 8 shows the SEM images of E. coli and S. aureus before and after antibacterial test. Fig. 8b reveals that the E. coli is seriously destroyed and half of the cell wall vanishes comparing to the Fig. 8a, indicating that the $Cu_2O$/cellulose composite gel has excellent antibacterial efficiency. Comparing to the morphologies of S. aureus before and after antibacterial test, Fig. 8d presents that the S. aureus is completely ruined. The SEM images demonstrates that the $Cu_2O$/cellulose nanofibers composite is more efficient against S. aureus than E. coli.

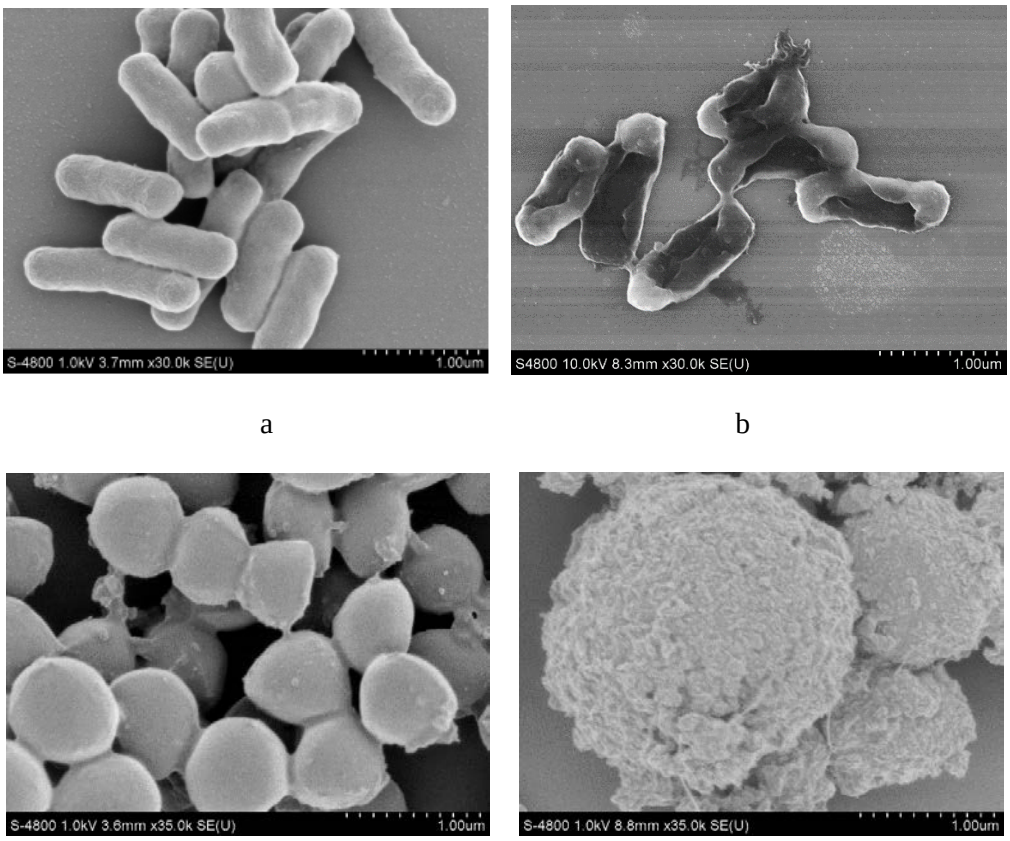


**Figure 8:** SEM images of E. coli before (a) and after (b) antibacterial test, and S. aureus before (c) and after (d) antibacterial test

### *3.6 Inductively coupled plasma (ICP)*

The $CuSO_4$ in solution could not absorbed by the cellulose nanofibers, and it is necessary to determine the content of $Cu_2O$/cellulose nanofibers composite. The test results of ICP-OES show that the content of Cu elementary is 11.6 w/w%, is to say that the content of $Cu_2O$ in composite is 13.1 w/w%, while the content of $Cu^{2+}$ ions in the solution is 1.25 w/w%, suggesting that the cellulose nanofibers can efficiently absorb the $Cu^{2+}$ ions and load high content $Cu_2O$ particles.

**Acknowledgement:** The authors are grateful to the financial support provided by the National key R&D Program of China (2017YFB0309400-2017YFB0309405) and Natural Science Foundation of China (Grant No. 51506075) and financial support from China Scholarship Council.

## References

**Chen, S. J.; Chen, X. T.; Xue, Z. L.; Li, L. H.; You, X. Z.** (2002): Solvothermal preparation of $Cu_2O$ crystalline particles. *Journal of Crystal Growth*, vol. 246, no. 1-2, pp. 169-175.

**Keskin, Z.; Urkmez, A. S.; Hames, E. E.** (2017): Novel keratin modified bacterial cellulose nanocomposite production and characterization for skin tissue engineering. *Materials Science & Engineering C-Materials for Biological Applications*, vol. 75, pp. 1144-1153.

**Khalid, A.; Khan, R.; Ul-Islam, M.; Khan, T.; Wahid, F.** (2017): Bacterial cellulose-zinc oxide nanocomposites as a novel dressing system for burn wounds. *Carbohydrate Polymers*, vol. 164, pp. 214-221.

**Khatami, M.; Heli, H.; Jahani, P. M.; Azizi, H.; Nobre, M. A. L.** (2017): Copper/copper oxide nanoparticles synthesis using Stachys lavandulifolia and its antibacterial activity. *IET Nanobiotechnology*, vol. 11, no. 6, pp. 709-713.

**Li, X.; Ni, C. H.; Yu, L. M.; Zhao, J.; Yan, X. F.** (2014): Synthesis, antibacterial activity and antifouling property of novel indole compounds containing acylamino groups. *Asian Journal of Chemistry*, vol. 26, no. 18, pp. 6253-6256.

**Ma, J. Q.; Guo, S. B.; Guo, X. H.; Ge, H. G.** (2015): Preparation, characterization and antibacterial activity of core-shell $Cu_2O$@Ag composites. *Surface & Coatings Technology*, vol. 272, pp. 268-272.

**Oh, S. Y.; Yoo, D. I.; Shin, Y.; Kim, H. C.; Kim, H. Y. et al.** (2005): Crystalline structure analysis of cellulose treated with sodium hydroxide and carbon dioxide by means of X-ray diffraction and FTIR spectroscopy. *Carbohydrate Research*, vol. 340, no. 15, pp. 2376-2391.

**Pang, H.; Gao, F.; Lu, Q. Y.** (2009): Morphology effect on antibacterial activity of cuprous oxide. *Chemical Communications*, no. 9, pp. 1076-1078.

**Pita, P. C. D.; Pinto, F. C. M.; Lira, M. M. D.; Melo, F. D. D.; Ferreira, L. M. et al.** (2015): Biocompatibility of the bacterial cellulose hydrogel in subcutaneous tissue of rabbits. *Acta Cirurgica Brasileira*, vol. 30, no. 4, pp. 296-300.

**Rezaie, A. B.; Montazer, M.; Rad, M. M.** (2017): Antibacterial, UV protective and ammonia sensing functionalized polyester fabric through in situ synthesis of cuprous oxide nanoparticles. *Fibers and Polymers*, vol. 18, no. 7, pp. 1269-1279.

**Sedighi, A.; Montazer, M.; Samadi, N.** (2014): Synthesis of nano $Cu_2O$ on cotton: Morphological, physical, biological and optical sensing characterizations. *Carbohydrate Polymers*, vol. 110, pp. 489-498.

**Sepulveda, R. V.; Valente, F. L.; Reis, E. C. C.; Araujo, F. R.; Eleoterio, R. B. et al.** (2016): Bacterial cellulose and bacterial cellulose/polycaprolactone composite as tissue substitutes in rabbits'cornea. *Pesquisa Veterinaria Brasileira*, vol. 36, no. 10, pp. 986-992.

**She, B. X.; Wan, X. J.; Tang, J. N.; Deng, Y. M.; Zhou, X. F. et al.** (2016): Size-and morphology-dependent antibacterial properties of cuprous oxide nanoparticle and their synergistic antibacterial effect. *Science of Advanced Materials*, vol. 8, no. 5, pp. 1074-1078.

**Sunada, K.; Minoshima, M.; Hashimoto, K.** (2012): Highly efficient antiviral and antibacterial activities of solid-state cuprous compounds. *Journal of Hazardous Materials*, vol. 235, pp. 265-270.

**Xiang, C. H.; Acevedo, N. C.** (2017): In situ self-assembled nanocomposites from bacterial cellulose reinforced with eletrospun poly (lactic acid)/lipids nanofibers. *Polymers*, vol. 9, no. 5, pp. 179-192.

**Xu, Y. Y.; Chen, D. R.; Jiao, M. L.; Xue, K. Y.** (2007): CuO microflowers composed of nanosheets: Synthesis, characterization, and formation mechanism. *Materials Research Bulletin*, vol. 42, no. 9, pp. 1723-1731.

**Xu, Z.; Yi, X.; Fen, X.; Liu, X. H.; Di, X.** (2003): Shape-controlled synthesis of submicro-sized cuprous oxide octahedra. *Inorganic Chemistry Communications*, vol. 6, no. 11, pp. 1390-1392.

**Yang, C. M.; Li, Q.; Lin, H.; Li, Y.; Xie, G. M.** (2016): Facile and eco-friendly fabrication of $Cu_2O$ truncated octahedral crystallites with enhanced antibacterial performance against Escherichia coli and Staphylococcus aureus. *Micro & Nano Letters*, vol. 11, no. 6, pp. 336-340.

**Zhang, F.; Tang, Y. B.; Yang, Y.; Zhang, X. L.; Lee, C. S.** (2016): In-situ assembly of three-dimensional $MoS_2$ nanoleaves/carbon nanofiber composites derived from bacterial cellulose as flexible and binder-free anodes for enhanced lithium-ion batteries. *Electrochimica Acta*, vol. 211, pp. 404-410.